Optimization and Antibacterial Response of N-Halamine Coatings Based on Polydopamine

Nadia Nazi, Adeline Marguier, Catherine Debiemme-Chouvy, Vincent Humblot

Article

Optimization and antibacterial response of *N*-halamine coatings based on polydopamine

Nadia Nazi[1,2], Adeline Marguier[3], Catherine Debiemme-Chouvy[2,*], Vincent Humblot[1,3,*]

[1] Sorbonne Université, Laboratoire de Réactivité de Surface UMR CNRS 7197, 4 place Jussieu, 75005 Paris, France
[2] Sorbonne Université, Laboratoire Interfaces et Systèmes Electrochimiques UMR CNRS 8235, 4 place Jussieu, 75005 Paris, France
[3] Institut FEMTO-ST UMR CNRS 6174, Université Bourgogne Franche-Comté, 15B Avenue des Montboucons, 25030 Besançon, France
* Correspondence: catherine.debiemme-chouvy@sorbonne-universite.fr (CDC), vincent.humblot@femto-st.fr (VH)

Abstract: Due to the ability of microorganisms first to adhere to material surface and then to lead to the formation of a biofilm, it is essential to develop surfaces having antimicrobial properties. It is well known that *N*-halamine coatings allow to prevent or minimize such phenomena. In the present work, various polydopamine (PDA) coatings containing chloramine functions are studied. Actually, three PDA-based films were formed by simple immersion of a gold substrate in a dopamine solution either at pH 8 in the presence or not of polyethyleneimine (PEI) or at pH 5 in the presence of periodate as oxidant. These films were characterized by polarization modulation reflection absorption infrared spectroscopy and X-ray photoelectron spectroscopy analyses and by scanning electron microscopy observations. The chlorination of these PDA films was performed by their immersion in a sodium hypochlorite aqueous solution in order to immobilize Cl(+I) into the (co)polymers (PDA or PDA-PEI). Finally, antibacterial assays towards a Gram-negative bacteria *Escherichia coli* (*E. coli*) and a Gram-positive bacteria *Staphylococcus epidermidis* (*S. epidermidis*) were conducted to compare the bactericidal properties of these three *N*-halamine coatings. Whatever the bacteria tested the PDA coating having the best antibacterial properties is the one obtained using periodate.

Keywords: polydopamine coating; *N*-halamine; antibacterial surfaces; XPS; PM-RAIRS; microbiological tests

1. Introduction

The fight against the adhesion and proliferation of bacteria on surfaces is a constant concern and a major medical and socio-economic issue for our society. In the medical and food industry, bacterial contamination of surfaces is responsible for many nosocomial and food infections through, among other things, prostheses, in operating theaters, in water pipe circuits or even in food industry installations [1-5]. In addition, this biocontamination of the surfaces may also lead to a deterioration of the structural and functional properties of the materials affecting the hulls of ships as well as civil engineering works or even cultural heritage [1, 6]. Treatments to fight against biocontamination of materials generate a significant economic impact and are sometimes ineffective, the biofilm lifestyle indeed conferring great resistance to microorganisms [7]. Thus, the prevention of bacterial adhesion appears essential and results in the development of antibacterial coatings as evidenced by the numerous research projects aimed at the development of such systems. One can cite surface functionalization with various antimicrobial molecules, such as enzymes, peptides, organic compounds (aldehyde, quaternary ammonium) or even oxide

protective layers [8-12]. Three main classes of antibacterial coatings can be designed in such a way: either to limit bacterial adhesion, which is called antiadhesive coatings and/or to inhibit the development of bacteria, these are said to be bacteriostatic films, or even to kill them as biocidal coatings [13]. These can act by contact and/or by release of antibacterial substances. Quaternary ammonium salts, silver ions or antibiotics are most often found in literature as biocidal substances incorporated or deposited on matrices, often polymeric, or chemically grafted on surfaces [14-18]. However, the increased resistance of microorganisms to these substances, the surrounding toxicity of these products and the complexity of grafting or deposition are obstacles to large-scale industrial use. Bio-based compounds such as enzymes or antimicrobial peptides have been considered as alternative routes but their high cost of production and purification, as well as their relative instability in the face of variations in pH or temperature, restrict their use [19-23].

As alternatives to these compounds, a class of antibacterial compounds, the *N*-halamines, has attracted great interest in recent years [24-26]. These compounds contain nitrogen-halogen covalent bonds which are formed by halogenation of imide, amide or amine groups. The antimicrobial properties of *N*-halamine compounds are due to the halogen which is at the oxidation state (+ I) and which therefore has oxidizing properties. It can react with suitable biological receptors such as thiol groups of amino acids within bacteria. This reaction can interfere with the metabolism of cells such as respiration, especially protein related processes, resulting in the death of the bacteria [24]. The disinfectant effectiveness of *N*-halamines is similar to that of bleach (sodium hypochlorite), but these compounds are more stable, less corrosive and relatively easy to generate. Indeed, after immobilization of the precursors (containing NH groups: primary or secondary amine, amide or imide functions) of *N*-halamine on a surface, they are converted into haloamine functions by a halogenation process (substitution reaction of H by Cl(+ I) or Br(+ I)), thanks to a sodium hypochlorite or a sodium hypobromite solution to generate chloramine or bromamine functions, respectively [24, 25, 27].

Various methods for bonding *N*-halamines to substrate surfaces have been described, however, these methods often require either complex surface pretreatment or lengthy coating formation procedures and often lack universality, strategies employed being specific to the physical and chemical properties of the surfaces of materials. In this context, polydopamine (PDA), an aqueous insoluble biopolymer produced by the 'auto-oxidation' of a catecholamine neurotransmitter, dopamine (DA), has become a highly studied polymer in materials science as a functional bio-system inspired used in a very wide range of applications. PDA provides exceptional adhesion properties producing a universal coating and offering the possibility of a large repertoire of post-functionalization, which has paved the way for many applications, both in the biomedical sciences and in the process, energy conversion or water treatment devices [28, 29].

In a previous study, we have demonstrated the possibility to elaborate a new antibacterial coating formed be a thin chlorinated PDA film [26]. This film is obtained by dopamine monomer polymerization in mild basic aqueous solutions followed by a treatment in sodium perchlorate (NaOCl) solution. This treatment leads to the formation of chloramine functions inside the polymer estimated between 10^{21} and 10^{22} at·cm^{-3} [26]. Microbiological tests towards *Escherichia coli* (*E. coli*) bacteria showed that chlorinated PDA coatings reduced *E. coli* adhesion up to 45 % compared to uncoated surfaces, while in the same time bacterial viability was reduced by 34% on chlorinated PDA coating compared to initial PDA films.

However, the maximum thickness obtained for a deposition of PDA in alkaline conditions in the presence of O_2 as oxidizing agent is less than 50 nm, which hinders any optimization of the antibacterial effect of the coating by increasing the thickness of the deposit in order to maximize the number of amine functions available. Moreover, many materials or molecules sensitive to pH, such as cellulose, polyester, phenolic resins, proteins or certain gels are not suitable for functionalization by dopamine in an alkaline

aqueous medium. At the end the fabricated PDA films are unstable in a strong alkaline environment [30-32].

To address those issues, various ways of optimizing the coating were considered during this study. First of all, increase the thickness of the PDA film by modifying the oxidant, replacing O_2 with sodium periodate which allows (i) deposition in an acidic medium with faster kinetics and (ii) to obtain thicker films [32]. The second path explored is based on the introduction of more amine functions through polyethyleneimine (PEI), forming a PDA-PEI composite. Moreover, amino-rich PEI has been frequently introduced as a cross-linking agent, which affords free-standing PDA/PEI composite films by Michael addition or Schiff base reaction and improves the chemical stability in strong alkaline environment [33]. This *N*-halamine based on co-deposition of PDA and PEI was studied and it was showed that the antibacterial ability of the coatings increased with increasing the PEI content. In addition, the chlorinated co-deposition coatings had significantly increased antibacterial properties compared to the unchlorinated ones, the chlorinated co-deposition coatings inactivating >99.99% of *Staphylococcus aureus* (*S. aureus*) and >99.9% of *E. coli* after contact of less than 10 min with PDA antibacterial materials [27, 34].

Thus, in the present work, the optimization of the synthesis of PDA coating containing chloramine functions was studied. For this purpose, first, the formation of three PDA-based films on gold surface was performed by simple immersion of the substrate in a dopamine solution either at pH 8.5 in the presence or not of PEI or in dopamine solution in the presence of sodium periodate as oxidizing agent at pH 5. Those films were characterized by polarization modulation reflection absorptions infrared spectroscopy (PM-RAIRS) and X-ray photoelectron spectroscopy (XPS) analyses and by scanning electron microscopy (SEM) observations. The chlorination of the PDA films was performed by immersion in a NaOCl aqueous solution in order to immobilize Cl(+I) oxidative species into the polymers. Finally, antibacterial assays against *E. coli* and *Staphylococcus epidermidis* (*S. epidermidis*) were conducted to compare the bactericidal properties of those *N*-halamine coatings.

2. Materials and Methods

Dopamine hydrochloride (98% purity), branched PEI (average M_W ~800 g·mol^{-1} by light scattering, average Mn ~600 motifs by gel permeation chromatography), sodium periodate (99.8% purity), tris-(hydroxylmethyl)aminomethane hydrochloride (Tris-HCl), sodium acetate (99% purity), and phosphate buffer saline (PBS) were obtained from Sigma-Aldrich (St-Quentin Fallavier, France). A house-hold bleach solution at 2.6% of active chlorine was diluted before being used for the chlorination of the PDA films. Ultra pure water was obtained from a Milli-Q system (Millipore, resistivity of >18 MΩ·cm^{-1}) from EMD Millipore Corp. (Billerica, MA, USA).

Glass substrates (11 mm × 11 mm) coated with a 5 nm-thick layer of chromium and a 200 nm-thick layer of gold were purchased from Arrandee (Werther, Germany). Before PDA coating, the gold-coated substrates were annealed in a butane flame to obtain a crystal reconstruction of the first atomic layers, and a UV−ozone cleaning procedure for 15 min was then applied prior to ultrapure water and absolute ethanol rinsing for a period of 10 min each [35].

PDA coatings

PDA-O_2

For the formation of the PDA coating, the substrates were immersed in dopamine solution, prepared by dissolving 0.5 mg·mL^{-1} of dopamine in 10 mM of Tris at pH 8.5. This PDA film deposition protocol was inspired by the protocol proposed by Messersmith group [36, 37]. Then, ultrasonic rinsing treatment in distilled water was carried out on the substrates for 1 minute; finally, the samples were dried with dry nitrogen. The samples are subsequently named PDA-O_2.

PDA-IO_4^-

For the deposition of PDA using sodium periodate ($NaIO_4$) as an oxidant at a concentration of 5 mM, the substrates were immersed in dopamine solution, prepared by dissolving 0.5 $mg \cdot mL^{-1}$ of hydrochloric dopamine in 50 mM sodium acetate at pH 5.5. This protocol was inspired by the study conducted by Ponzio *et al.* [32]. Subsequently, the substrates were washed with ultrapure water for 5 minutes under sonication and then dried with dry nitrogen. The samples are subsequently named PDA-IO_4^-.

PDA-PEI

The deposition of the PDA-PEI composite was carried out by immersing the substrates in a solution formed from a mixture of dopamine at 0.5 $mg \cdot mL^{-1}$ and PEI at 0.25 $mg \cdot mL^{-1}$ in 10 mM of Tris at pH 8.5, under stirring. This PDA-PEI composite film deposition protocol was inspired by the study conducted by Xu *et al.* [33]. This functionalization is followed by ultrasonic treatment of the substrates in ultrapure water and followed by drying with dry nitrogen. The samples are subsequently named PDA-PEI.

PDA film chlorination

For chlorination, PDA-XX films were soaked in 1 or 10 mM NaOCl solution at pH 10, at room temperature [26, 38, 39]. After chlorination, the substrates were washed with deionized water thoroughly and nitrogen-dried. After chlorination, the coatings are named PDA-XX-Cl.

Polarization Modulation Reflection Absorptions InfraRed Spectroscopy (PM-RAIRS)

PM-RAIRS measurements were carried out on a Nicolet Nexus 5700 Fourier-transform infrared (FT-IR) spectrometer (Madison, WI, USA) equipped with a wide-band HgCdTe detector cooled with liquid nitrogen. Infrared spectra were obtained by addition of 128 scans at 8 cm^{-1} resolution. A ZnSe photoelastic modulator and a ZnSe grid polarizer were placed prior to the sample to modulate the incident beam between p and s polarizations (PM90, HINDS Instruments, Inc., Hillsboro, OR, USA), the modulation frequency was 36 kHz. Interferograms (sum and difference) were processed via Fourier transformation to obtain the resulting PM-RAIRS signal, which is the differential reflectivity:

$$\Delta R/R^0 = (Rp - Rs)/(Rp + Rs) \quad (1)$$

with R^0 is the reflectivity of the initial IR beam and R the one after reflexion on the substrate; Rs and Rp are the signals perpendicular and parallel to the incident plane, respectively.

X-ray photoelectron spectroscopy (XPS)

XPS analyses were performed using an Omicron Argus spectrometer (Taunusstein, Germany) equipped with a monochromated Al Kα X-ray source ($h\nu$ = 1486.6 eV) working at an electron beam power of 300 W. Photoelectron emission was analyzed at a take-off angle of 45°. The analyses were carried out under ultrahigh vacuum conditions (≤10^{-10} Torr) after introduction via a load lock into the main chamber. Spectra were obtained by setting up a 100 eV pass energy for the survey spectra, and a pass energy of 20 eV was chosen for the high-resolution regions. Element peak intensities were corrected by Scofield factors [40]. CasaXPS software (Casa Software Ltd., UK) was used to decompose XPS spectra using a Gaussian/Lorentzian ratio of 70/30.

Water Contact Angle (WCA)

Static water contact angles (DSA100 apparatus, Krüss, Hamburg, Germany) were measured under ambient conditions (at 20°C and 40% relative humidity) by analyzing the

profile of sessile drops (1 µL droplet of milliQ water) deposited on a given surface. The drop profile was recorded by a CCD camera, while the angles were measured by the image analysis software. For each analyzed surface, at least for different location were chosen for the deposition of the droplet; each test was performed in triplicate on three different samples. The reported values for a given surface are thus the averages of these 36 measurements.

Chemical 5-thio-2-nitrobenzoic acid (TNB) titration

The presence of chloramine functions was confirmed by measuring the bleaching of a 5-thio-2-nitrobenzoic acid (TNB) solution at 412 nm [41]. Fresh TNB solution was produced before each experiment via addition of 2 equivalents of cysteine (Cys) to 1 equivalent of 5,5′-dithiobis(2-nitrobenzoic acid) (DTNB) following the reaction:

$$\text{DTNB} + 2\ \text{Cys} \rightarrow 2\ \text{TNB} + \text{cystine} \qquad (2)$$

For this aim, in equal volumes, 2×10^{-3} M cysteine and 10^{-3} M DTNB were mixed in 50 mM phosphate buffer solution (PBS) at pH 7.4, giving a highly colored yellow/orange solution [42]. Then, this stock solution was diluted 10-fold with 50 mM PBS, pH 7.4. The different substrates were immersed in this solution for 24 h. The yellow-colored TNB reacts with haloamine functions to regenerate colorless DTNB. The UV/visible absorbance measurements were carried out using a spectrometer with 1 cm path length cuvettes. According to Beer−Lambert's law, the density of chloramine functions (d_{Cl}), in at·cm^{-3}, was calculated according to the following equation:

$$d_{Cl} = \frac{A_{PDA} - A_{PDA-Cl}}{2\,\varepsilon\,l\,V_{coating}}\,V_{TNB}\,N_A \qquad (3)$$

where A_{PDA} and $A_{PDA\text{-}Cl}$ are the absorbance of the TNB solution containing the substrate with the PDA coating and with the chlorinated PDA coating, respectively; ε is the molar absorptivity coefficient of TNB, ε = 14,100 M^{-1}·cm^{-1}, l is the length of the spectrometer cuvette and is equal to l = 1 cm, $V_{coating}$ is the volume of the PDA film in cm^3, V_{TNB} is the volume of the TNB solution in L and N_A is Avogadro's constant.

Microbiological tests

Microbiological experiments were conducted with *Escherichia coli ATCC 25922* described as a rod shape with an average height of 1 µm and *Staphylococcus epidermidis* CIP 6821 described as a sphere ranging from 1 to 2 µm diameter. *S. epidermidis* strain was chosen as non-pathogenic bacteria mimicking *S. aureus* bacteria. Three culture media were used for these experiments: 2 nutritive media, Lysogeny-broth medium (LB) for *E. coli*, Muller-Hilton medium (MH) (Sigma-Aldrich, St-Quentin Fallavier, France) for *S. epidermidis* and a un-nutritive phosphate buffer saline (PBS) medium for killing experiments.

Bacteria were stored at −80°C. Before the tests, they were incubated overnight on LB agar plate for *E. coli* and MH agar plate for *S. epidermidis*, at 37°C. Then, a liquid pre-culture was prepared with one colony of *E. coli* or *S. epidermidis* in LB or MH media, respectively, and incubated for 18 h at 37°C under stirring (90 rpm). Bacteria were then harvested by centrifugation (3500 rpm, 4°C, 20 min). Bacteria were re-suspended in the PBS medium and bacterial suspensions were adjusted to an absorbance at 620 nm of 0.01 ($5\text{x}10^6$ CFU·mL^{-1}).

Bacteria Growth Capacity (Cultivability of Adhered Bacteria)

Bacterial growth capacity after contact with functionalized surfaces was determined performing killing tests. Before bacterial inoculation, the surfaces were disinfected by washing them five times with ethanol solution at 70%. The killing test was performed in sandwich configuration. For this, 20 µL of the bacterial suspension in PBS media were deposited on a first plate; then, a second plate was placed onto the first one, on the coating side so that the bacterial suspension is sandwiched between the two substrates. After 3 h of contact, at room temperature, the surfaces were mildly rinsed with sterile PBS in order to remove non-adhered bacteria, then transferred into a tube containing 2 mL of sterile PBS solution and sonicated (Bandel in Sonorex RK 31, Berlin, Germany; f= 35 kHz and P= 90 W) for 2 min to recover the adhered bacteria without damaging them. After the sonication, SEM observations of the plates were performed to verify that most of the adhered bacteria were detached during the sonication process. Traditional dilution/counting was carried out in in triplicate on LB or MH agar plates. The plates were incubated at 37°C overnight before enumeration. Results were expressed in the number of attached and cultivable bacterial cells onto the different surfaces per mL (CFU·mL^{-1}). The percentage of killing *(%killing*) was calculated using equation (4):

$$\%killing = 100\ (CFU_{ref} - CFU_{chlorinated\ surface})/CFU_{ref} \quad (4)$$

Each test was done in triplicate, and the number of CFU·mL^{-1} is the average of the results obtained for each sample.

Epifluorescence optical microscopy observations

Samples were immersed in 4 mL of bacterial suspension and incubated for 3 h at 37°C. It is important to keep in mind that this incubation time corresponds to the limit of the reversible phase in the biofilm formation process. Surfaces were then thoroughly and carefully rinsed 8 times by replacing 1 mL of the bacterial suspension by 1 mL of fresh PBS solution to remove non-attached bacteria. Adhered bacteria on the surfaces were fluorescently stained by adding 1 µL of 5x10^{-3} M Syto9® (Invitrogen, US) solution and 3 µL of 5x10^{-3} M Propidium Iodide® (Invitrogen, US) solution and were incubated for 15 min at 37°C .

Then the surfaces were directly observed in the last rinsing solution by using the fluorescence/reflection mode of an upright epifluorescence microscope (Axio Observer, Zeiss) equipped with a long working distance water objective (W Plan-Apochromat 63X/1.0, working distance 2.0 mm, Zeiss®). On each surface, micrographs were taken on 10 random locations. Experiments were conducted with two surfaces of each type and reproduced by 3 independent experiments. Micrographs were analyzed by ImageJ V.1.44d software® (NIH). Each image was processed to select the color channel and adjust thresholds by Otsu or Intermodes method depending on the intensity histogram of each image. Then, the number of adhered bacteria (N) and their size on each micrograph were calculated with help of the analyze particle plug-in. The *%killing* was calculated using equation (5):

$$\%killing = 100\ (N_{green\ +\ red\ bacteria} - N_{red\ bacteria})/N_{green\ +\ red\ bacteria} \quad (5)$$

The significance of two-by-two differences between averages cells number in the diverse culture conditions was evaluated by bilateral Student's t tests (application conditions: independent data and equal variances assessed by F-test) with significance thresholds of 0.01 and 0.05. The alternative hypothesis ($\mu_1 \neq \mu_2$) was assumed to be true when the main hypothesis ($\mu_1 = \mu_2$) was rejected, where µ1 and µ2 are the two mean values to be tested for significant difference.

3. Results

3.1. PDA Coating Elaboration

In aerated solution, dopamine monomers are known to self-polymerize upon oxidation within the right concentration and pH conditions. The polymerization is usually accompanied with a change of the solution color from colorless to dark brown [26]. In this study, we have studied several ways of obtaining PDA films by changing the oxidant agent, atmospheric O_2 or sodium periodate, or by adding a small polymer, PEI, which is known as a good reticulate agent [34, 43].

The DA polymerization was followed upon increasing contact time between the gold substrates and the DA solutions (Figure S1). Figure 1 presents the PM-RAIRS data obtained for the three routes of PDA grafting, showing similar profile. According to previous study on the formation of PDA films using atmospheric O_2 as oxidant [26], in Figure 1(a) a broad IR massif is observed in the 1600 cm^{-1} region, with a second group of features is visible at lower wavenumbers. These IR features indicate the presence of a PDA film, with the main characteristic peaks observed at 1620 and 1515 cm^{-1}, assigned to the stretching of the (C=C) group within the DA ring together with the stretching ν(N−H) vibrations [44], respectively. In the second region, IR peaks are observed at 1450, 1350, and 1290 cm^{-1}, respectively assigned to the stretching vibrations (C-N-C) of the DA ring and to free catechol moieties of free dopamine, ν(C−O) and ν(C=N). These PM-RAIRs features are consistent with the formation of PDA coating on gold surface [44-47].

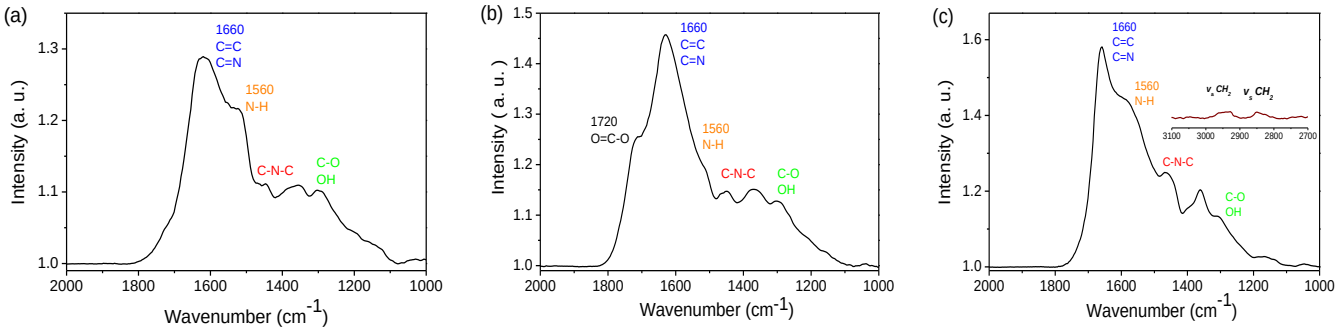

Figure 1. PM-RAIRS spectra of gold surface coated with (**a**) PDA-O_2, (**b**) PDA-IO_4^-, **(c)** PDA-PEI.

PM-RAIRS analyses of the spectrum obtained using periodate is presented in Figure 1(b); the spectrum obtained after 5 hours reveals the same characteristic groups of PDA observed previously for the PDA-O_2 film at 24 hours. However, one can also note that a new peak appears at 1720 cm^{-1} assigned to the stretching vibration of a C=O bond of a carboxylic group. This peak suggests a hyper oxidized state of the PDA due to the strong oxidizing power of periodate, the material is probably richer in carboxylic group or quinonoid structures and has undergone a partial loss of carbon [31]. This is in accordance with the known chemistry of periodate, which, when used in excess, can cause *o*-quinone oxidative cleavage [48]. The spectrum obtained for the PDA-PEI film after 24 hours, Figure 1(c), is also similar to the one obtained for PDA-O_2. In addition, IR features are also observed in the 2800-2900 cm^{-1} region, assigned to the stretching vibration of CH_2 groups from the PEI backbone. Finally, it is important to note that the intensity of the N-H vibration at 1560 cm^{-1}, compared to the C-C, C=N at 1660 cm^{-1} is greater in the latter case, suggesting the presence of more NH groups in the case of the PDA-PEI film [34].

PDA film growth can be quantitatively investigated using PM-RAIRS data, by integrating the area under the IR features as a function of immersion time (Figure S1), as presented in Figure 2. Growth profiles observed are quite different for all three polymerization routes. For PDA-O_2 films, a rapid increased of the peak's intensity is observed for the 12 first hours, followed by a slowest increase to end up to a plateau after 48 hours. This stationary phase can be attributed to the depletion of the monomer in the supernatant solution, being able to crosslink on the PDA film, in favor of non-reactive quinone molecules [49]. The ellipsometry data (Figure S2B) confirms the logarithmic kinetic deposition profile obtained by PM-RAIRS analysis. On the contrary, PDA-IO_4^- films show an even faster increase of the IR intensity during the first 3 to 5 hours to quickly stabilize into a plateau regime. The thickness measurements obtained by SEM (Figures S2A and S3) also confirm the deposition kinetics observed by PM-RAIRS, indeed a faster deposition kinetics than during a conventional deposition is observed, for this a logarithmic kinetics is observed. Finally, the data obtained for PDA-PEI film seems to be a mix of both previous ways, with a fast increase during 5 hours, smaller than for PDA-IO_4^- though, followed by a slowest increased up to a steady-state obtained after 10 hours of immersion. It is important to note that the intensity of the areas under peaks are expressed in arbitrary units; thus, a calibration was applied using the thickness obtained on the plateau regime using ellipsometry analysis and SEM observations [26] (Figures S2 and S3), showing similar thicknesses for both PDA-O_2 and PDA-PEI around 50-55 nm and 60-65 nm, respectively, while for PDA-IO_4^- the film thickness reaches 110-115 nm [32]. Thus, one can conclude on the strong efficiency of periodate as oxidant agent compared to atmospheric O_2, leading to greater thickness of PDA films, together with faster growth rate. Consequently, the use of periodate allows to accelerate the oxidation kinetics of dopamine, after 5 hours of immersion a thickness plateau around 100 nm is reached, i.e. a gain of 60 nm in thickness compared to the conventional deposit obtained after 24 h. Besides, copolymerisation of PDA and PEI leads to similar thickness of the film than PDA-O_2 one, with a kinetic growth rate increased by a factor 2 in the case of PDA-PEI, with the hypothesis of a greater concentration of NH groups.

Contact angle measurements with water were used to assess the wettability of a surface and to demonstrate a change in the chemistry of the latter following surface modification (Figure S4). It is noted that for the PDA-O_2 coating, the contact angle decreases over time to reach a plateau after 3 h of deposition, level around 55° which approaches the value of the contact angle reported in the literature [32]. It can thus be seen that this monitoring of wettability makes it possible to have, in a simple and rapid way, an indication of the time at the end of which the coating becomes homogeneous at the macroscopic level in terms of coverage of the substrate and thus completes the monitoring by PM-RAIRS and ellipsometry.

Concerning PDA-IO_4^-, the evolution of the contact angle formed between the coating and the water matches the profile obtained for the PDA-O_2 coating. In fact, a sharp reduction in the angle is observed during the first 10 hours, then a plateau is observed indicating the presence of an homogeneous coating on the gold surface. Note that this change is similar to the profile found when monitoring the thickness of the deposit. Thus, just as with the PDA-O_2 coating, the kinetic monitoring of the deposit by measuring the contact angle turns out to be a simple method of monitoring the PDA deposit over time. Finally, it is noted that PDA-O_2 and PDA-PEI composite have the same evolution profile of wettability during the first 30 hours of deposition. Indeed, the contact angle with water decreases over time to reach a plateau after 5 hours of deposition, around 50° which is slightly lower than the value obtained from pure PDA.

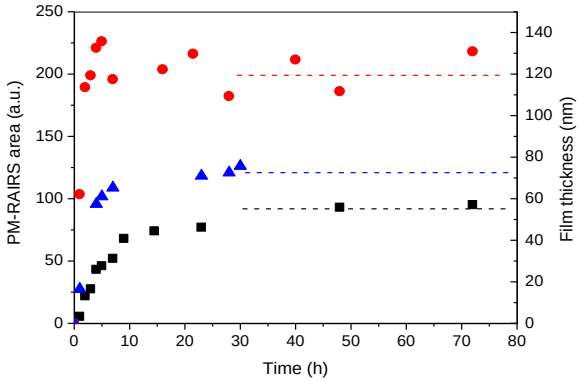

Figure 2. PDA film growth. PM-RAIRS peak area (left axis) and film thickness (right axis) *vs.* immersion time in DA solution. Data are from Figure S1, S2 and S3. Square: PDA-O_2. Circle: PDA-IO_4^-. Triangle: PDA-PEI.

XPS analyses were performed on these three sets of the PDA-coated Au surface, the survey spectra are presented in Figure 3. For all samples, the photopeaks C1s (285 eV), O1s (530 eV), and N1s (400 eV) are observed, whereas the Au4f contribution (84 eV) is not detected confirming film thickness greater than 15 nm [50]. In addition, for PDA-IO_4^-, the I3d signal, at 620-630 eV, is observed together with the counter-ion Na^+ signal at 1051 eV. For samples PDA-O_2 and PDA-IO_4^-, the chemical composition in carbon and nitrogen is close to the theoretical composition of PDA (N/C = 0.125) taking into account the carbon contamination, which slightly reduces the N/C ratio (Table 1). Finally, for the PDA-PEI sample, the atomic percentage of N is much greater than for the two others films, due to the presence of PEI as copolymer in the film, with the N/C ratio being accordingly twice bigger than previously.

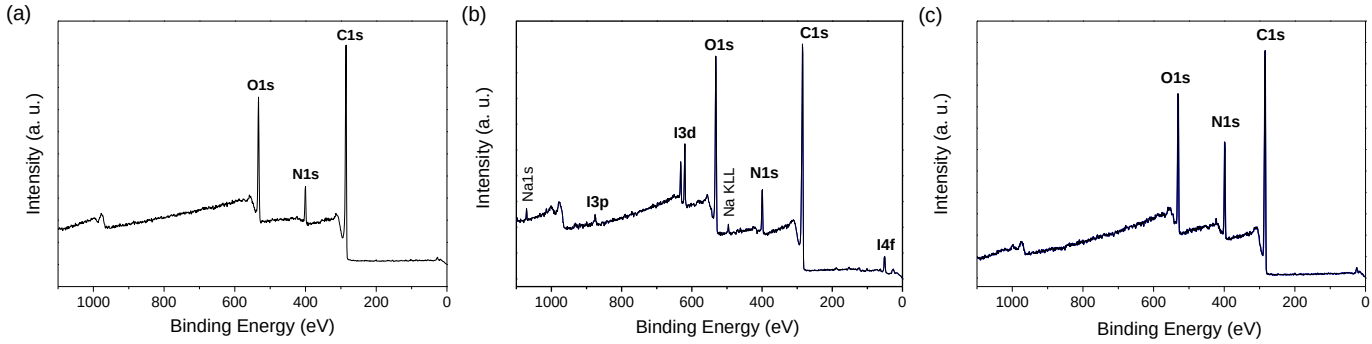

Figure 3. XPS survey spectra of gold surface coated with (a) PDA-O_2, (b) PDA-IO_4^- and (c) PDA-PEI.

Table 1. Atomic percentage and N/C ratio obtained from XPS data.

	C	N	O	Au	I	Na	N/C
PDA-O_2	75.5	7.3	17.2	ND	-	-	0.1
PDA-IO_4^-	72.2	7.1	19.3	ND	0.9	0.5	0.1
PDA-PEI	69.4	15.4	15.2	ND	-	-	0.2

[1] ND=non detectable

3.2. PDA Coating Chlorination

The chlorination of the different PDA films was carried out using diluted NaOCl as a function of contact time and concentration in order to optimize the chlorination process. Figure 4 shows the evolution of the PM-RAIRS spectra upon increasing contact time between the PDA films and the NaOCl solution. Two concentrations of the NaOCl solutions were tested, 1 and 10 mM. After a certain time, drastic changes on the profile spectra can be observed suggesting the degradation of the film as long contact time with alkaline solution can degrade the polymer structure [38, 51, 52]. It is first observed that after the chlorination, a change in the IR spectra of the three PDA films is observed. In fact, the latter appear to show a strong decrease in the peak at 1515 cm^{-1}, a peak attributed to the deformation vibration of the δ(N-H) amine bond, therefore suggesting the creation of chloramine functions. There is also a shift in the peak characteristic of the aromatic cycle from 1620 cm^{-1} to 1645 cm^{-1}. This change can be a consequence of the grafting of chlorine atoms on nitrogen atoms located near the aromatic ring modifying the chemical environment of the latter. Finally, the appearance of a shoulder around 1720 cm^{-1}, the intensity of which increases with the chlorination time (Figure 4) may be ascribed to the appearance of carboxylic functions due to the oxidation of the PDA coating on contact with hypochlorite ions.

For instance, on PDA-O_2 films, Figure 4(a,d), the intensities of the peaks of the chlorinated spectra start to decrease for contact time of 15-20 minutes, with a complete destruction of the film after 50 minutes of contact time with NaOCl solution. Thus, an optimized contact time for the chlorination process for PDA-O_2 was chosen to be 20 minutes at 1 mM. The same processes were applied for the PDA-IO_4^- and PDA-PEI films, Figure 4(b,e) and (c,f), ending up with optimized chlorination times of 20 minutes at 1 mM and 10 minutes at 10 mM respectively.

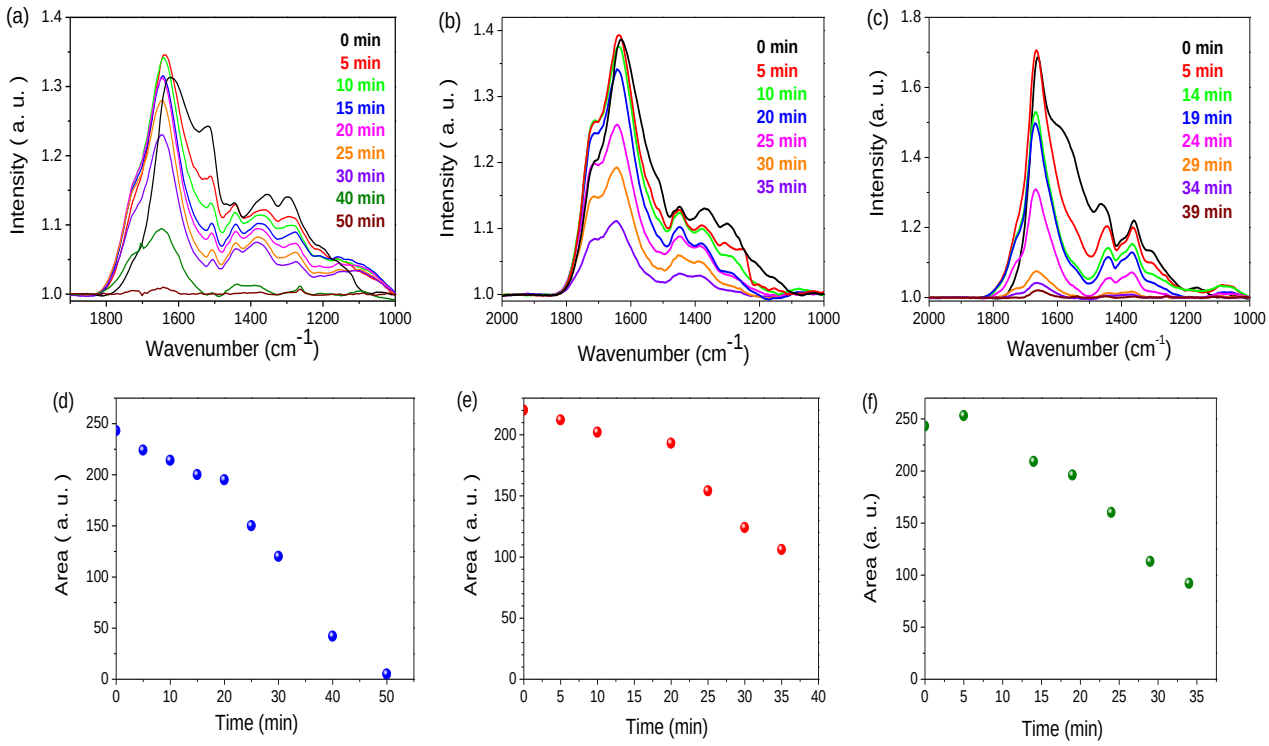

Figure 4. Chlorination of PDA films as a function of immersion time in (a),(b) 1 mM, (c) 10 mM NaOCl solution. (a),(b),(c): PM-RAIRS spectra. (d),(e),(f): area under IR peaks. (a),(d): PDA-O_2 ; (b),(e): PDA-IO_4^- ; (c),(f): PDA-PEI.

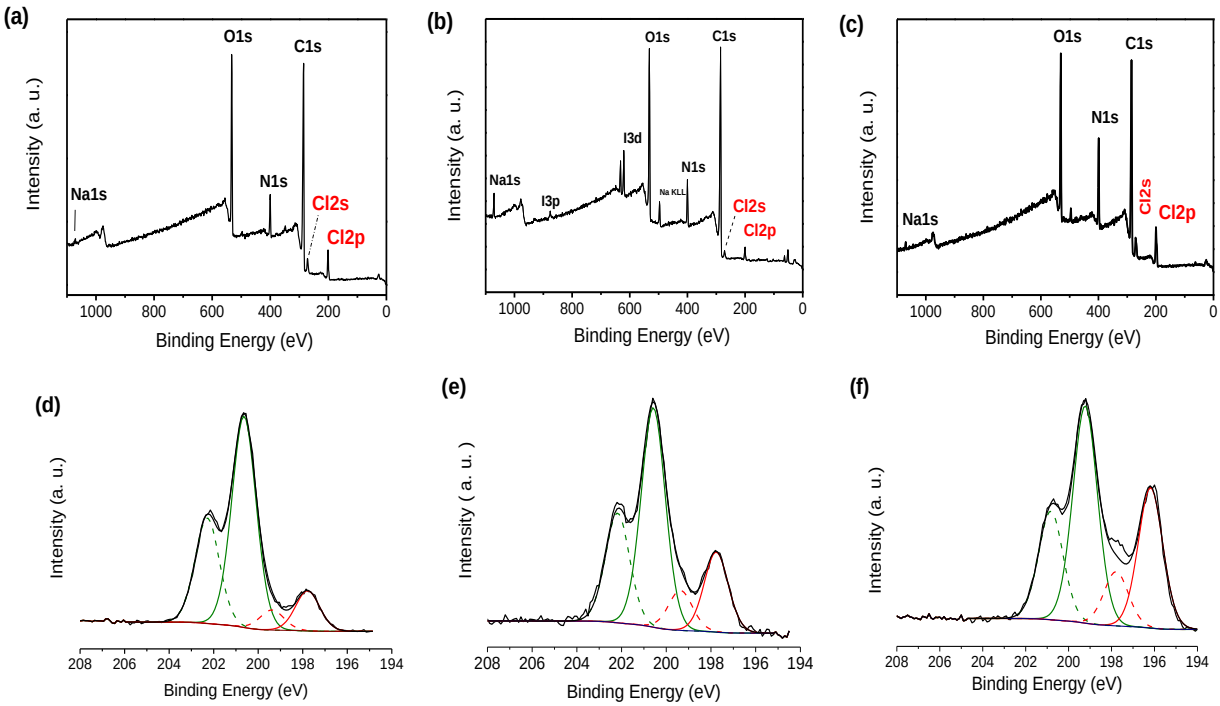

Figure 5. XPS survey spectra (a-c) and high resolution Cl2p spectra (d-f) after chlorination of (a, d) PDA-O_2, (b, e) PDA-IO_4^- and (c, f) PDA-PEI.

XPS experiments were carried out for the different PDA films chlorinated with optimized conditions, the data are presented in Figure 5 and the quantitative data are summarized in Table 2.

First, the survey spectra in Figure 5 (a-c) show additional contributions at 200 eV and 270 eV, assigned to Cl2p and Cl2s contributions, respectively, confirming the successful chlorination of the PDA films. High resolution spectra of the Cl2p contribution are also shown in Figure 5 (d-f), exhibit two distinct doublets centered for the $Cl2p_{3/2}$ contribution around 200 eV and 198 eV. The most intense one, at 200 eV, named Cl_{200}, is usually assigned to chlorine atoms in N-Cl bond, while the lower binding energy one is ascribed to free chlorine atoms. Thus, one can first conclude that the chlorination process was successful, and second that only a few amount of free Cl atoms remain at the surface even after heavy rinsing procedure. It is interesting to note, that the amount of Cl_{200} differs from one film to another, thus both PDA-O_2 and PDA-PEI exhibit N atomic percentages about 4.0%, while PDA-IO_4^- film shows only 2.7%. However, *per se*, such analyses are not sufficient to conclude that one film or another contains the highest amount of haloamine functions. In fact, one should consider the original amount of N1s atoms present in the analyzed thickness of the films, and it is possible to calculate the percentage of chlorinated NH groups by looking at the Cl_{200}/N ratio. From Table 2, it can be concluded that the efficiency of chlorination is the best for the PDA-O_2 film with more than 60% of the N atoms that are chlorinated, while this value is only 30% for the 2 others PDA films.

These results thus only give us information on the composition of the surface of the coating one (10-15 nm of thickness probed). These differences between the PDA-O_2, PDA-IO_4^- and PDA-PEI coatings can be explained by the availability of N-H functions. Indeed, let us recall that for the PDA-IO_4^- coating, acid conditions and a strong oxidant were used to generate the PDA film, generating a different hyperoxidized structure compared to the PDA-O_2 film, with a higher proportion of tertiary amine functions which does not allow their chlorination. For the PDA-PEI coating, this drop in N-Cl can be due to the fact that N-H functions could be engaged in hydrogen bonds with the adjacent catechol functions which do not allow the chlorination of these amine functions, Figure S5.

Table 2. Atomic percentage and ratio obtained from XPS data for PDA coatings after chlorination.

	C	N	O	I	Au	Na	N/C	Cl_{total}	Cl_{200}	Cl_{200}/N
PDA-O_2-Cl	69.85	6.45	18.9	-	-	-	0.1	4.8	4.0	0.6
PDA-IO_4^--Cl	69.2	6.5	20.0	0.7	-	1.3	0.1	2.3	1.7	0.3
PDA-PEI-Cl	61.4	13.7	16.4	-	-	0.8	0.2	7.7	4.5	0.3

Finally, it is possible to obtain the Cl/N ratio in the whole PDA film, not only from the extreme surface as shown previously by XPS. In order to do that, a chemical dosage using the oxidative properties of the chloramine film, to follow the oxidation of TNB into the corresponding dimer DTNB, accompanied with a change of color of the solution, Figure S6. Thus, by measuring the optical density at 412 nm, the amount of Cl(+I) immobilized in the PDA film can be determined. The results are reported in Table 3, together with the density of chlorine atoms for each film. The film having the highest density of Cl(+I), hence N-Cl groups, is the PDA-PEI film. None the less, all three films of PDA exhibit high amount of chlorine, ranging from $5x10^{20}$ to almost 10^{22} at·cm^{-3}.

This clear difference between XPS results and chemical assay with TNB comes first of all from the fact that a quantification technique is used here which probes the depth of the layer, unlike the XPS analysis which only gives information, as a reminder, on the coating surface. In addition, the nature of the reagent used and the nature of the PDA-IO_4^- coating which are rougher and denser than the PDA-O_2 coatings Figure S3 can explain this difference. Indeed, TNB being a bulky molecule would make its infiltration over the entire thickness of the coatings difficult.

Table 3. TNB solution absorption (A) at 412 nm after 24 h of immersion of various samples, the number of chlorine atoms, density (Equation 3) of chloramine in PDA-O_2, PDA-IO_4^- and PDA-PEI coatings estimated by TNB dosage, and the Cl_{200}/N atomic ratio considering a N density of $5.3x10^{21}$ at·cm^{-3}.

	A at 412 nm	Cl (at.)	d_{Cl} (at·cm^{-3})	Cl_{200}/N
PDA-O_2-Cl	0.30	$4.0\ 10^{16}$	$2.5\ 10^{21}$	0.47
PDA-IO_4^--Cl	0.50	$5.8\ 10^{15}$	$5.0\ 10^{20}$	0.10
PDA-PEI-Cl	0.20	$9.25\ 10^{16}$	$9.25\ 10^{21}$	0.29

3.3. Antibacterial properties of chlorinated PDA surfaces

Several microbiological tests have been performed in order to evaluate the different antibacterial activities of the chlorinated PDA coatings. These tests were performed with *E. coli* ATCC 25922 and *S. epidermidis* CIP 6821. They were carried out following two routes: a direct one by optical microscopy using fluorescent stains to evaluate the bacterial adherence and the cell mortality; a second indirect route was based on the recovery of adhered bacteria and viable cell culture counting on agar plates.

The first test was carried out in order to evaluate the adhesive properties of PDA-XX and PDA-XX-Cl coatings towards bacterial suspensions, the main results are presented in Figure 6. The total adhered flora was evaluated by counting the green bacteria present on the surface after recording several areas on the different surfaces; this green fluorescence was obtained by marking bacteria with Syto™ 9 fluorescent staining, that penetrates all living and damaged bacteria. The numbering of adhered bacteria was done using ImageJ software. Looking first at the results for *E. coli*, Figure 6(a), one can notice that all chlorinated surfaces exhibit a decreased number of bacteria compared to the respective non-chlorinated surfaces. Hence, for PDA-O_2 and PDA-IO_4^-, the net decrease of bacterial adherence is 25% and 38%, respectively, with significant statistical differences ($p < 0.01$),

see Figure S7. Concerning the PDA-PEI surface, a decrease of 21% is observed, Figure 6(a) but with no significant difference ($p > 0.01$), Figure S7. Surprisingly, so such tendencies were observed for *S. epidermidis* bacterial strain, Figure 6(b). All the adherence recorded show no statistically significant differences, meaning that the chlorine substitution does not affect the contact between the surface and the bacterial membrane. This can be probably explained by the composition of the membrane of Gram positive bacteria compared to the one of Gram negative bacteria, with the absence of charged liposaccharide in the membrane in the latter case. In addition, only one relevant statistical difference is observed in the case of PDA-PEI surfaces, which exhibit a much lower adherence compared to its chlorinated counter-part, with 36% less adhered bacteria. This could be explained again by the specific positive charges present on the outer membrane of the Gram positive bacteria, resulting on charged repulsion between this one and the positively charged amine groups of PEI under physiological conditions [53].

Following the evaluation of total adherence properties by recoding green fluorescent bacteria on the various surfaces, a second fluorescent staining was introduced in the system and microscopy images were again recorded. This second fluorescent stain,

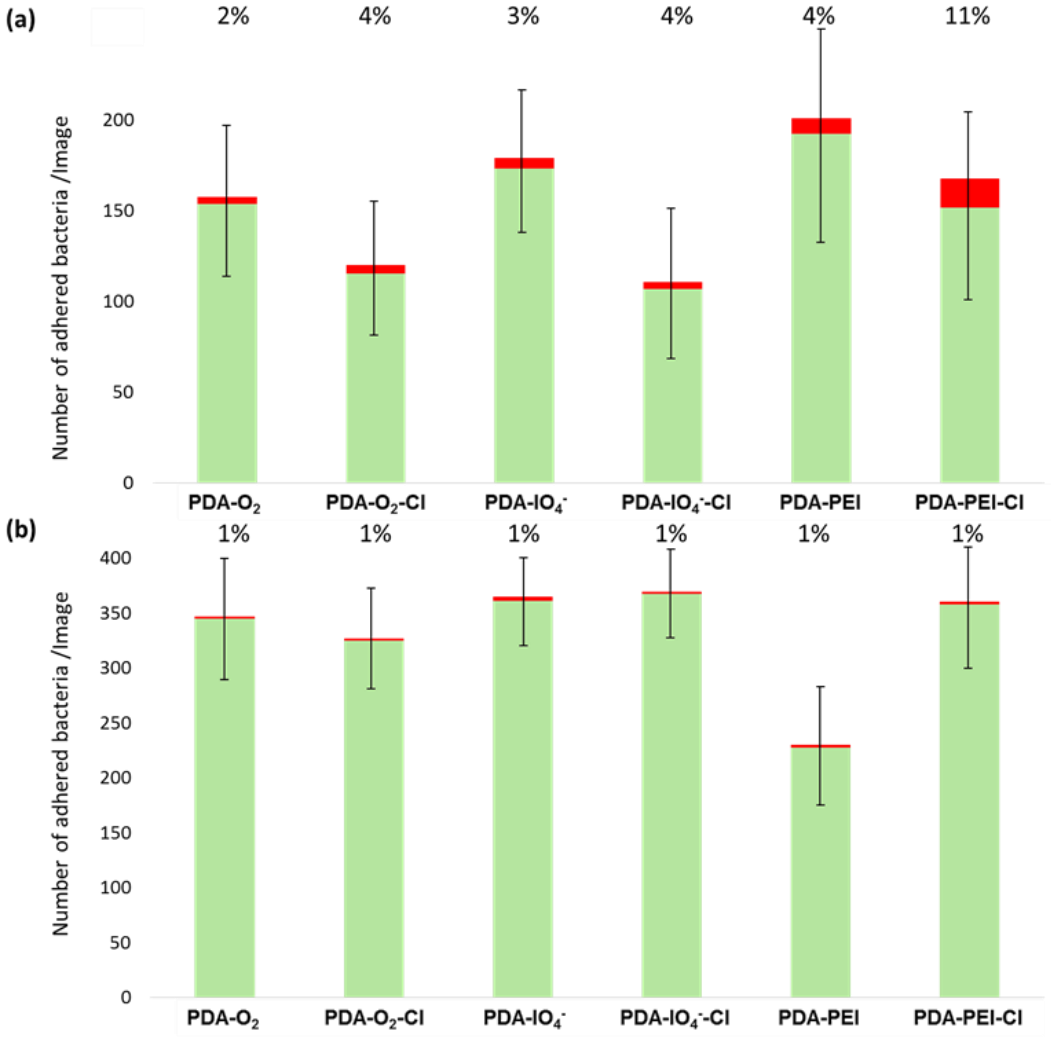

Figure 6. Mean number of adhered bacteria observed by optical microscopy (green bars) and % killing obtained from fluorescence optical microscopy (red bars) for (a) *E. coli* and (b) *S. epidermidis* and for the three PDA coatings before and after chlorination.

propidium iodide, penetrates only damaged bacterial membranes, and thus allows to evaluate the killing properties of surface using equation (5).

The results are presented in Figure 6 (red bars on top of green ones) for the six studied surfaces and for both Gram negative and positive bacterial strains, presenting the numbers of red bacteria recorded compared to the number of green bacteria recorded on the same surface. For each surface, the percentage of killing is also indicated on the charts. First of all, one can notice the very low killing efficiency obtained with this technique for all surfaces, with less than 1% of killing on average for all PDA coatings towards *S. epidermidis*, Figure 6(b), and a killing efficiency comprised between 2 and 11% towards *E. coli*, Figure 6(a). It is also important to notice, that with this live/dead fluorescent technique, one can evaluate the killing properties of surfaces without the bactericidal molecules, for instance the fact that a PDA-PEI surface exhibits a 4% killing property towards *E. coli* bacteria, to be compared with the 11% obtained once the PDA-PEI coatings has been chlorinated, Figure 6(a). These results may be surprising when compared with those reported in literature: for instance with PDA-PEI-Cl coating, Chien *et al.* have shown a 99.99% of killing towards *S. aureus* and 99.9% towards *E. coli*, but these results were obtained using an indirect method, *ca.* CFU numbering on agar plates [34].

However, it is known also from literature, that the live/dead fluorescent techniques are very efficient when the damaged caused to the bacteria by the antibacterial agents affect directly the integrity of the membranes of the bacteria. In addition, the mode of actions of haloamines moieties remains unclear, and seems to be more directed towards growth inhibition by blocking of the cellular division than membrane disruption, that could explain the poor number of red bacteria in our fluorescent optical microscopy experiments. Indeed, the contact-active antibacterial mechanism inactivates the growth bacteria by remaining bound to surfaces. The mechanism involves the direct transfer of an oxidizing halogen from *N*-halamine to bacterial cells. Halogen has a strong tendency to combine with another element, inhibiting the priming process of bacterial cells. In this way, the antibacterial action occurs without the dissociation of the halogen from haloamine bonds [54].

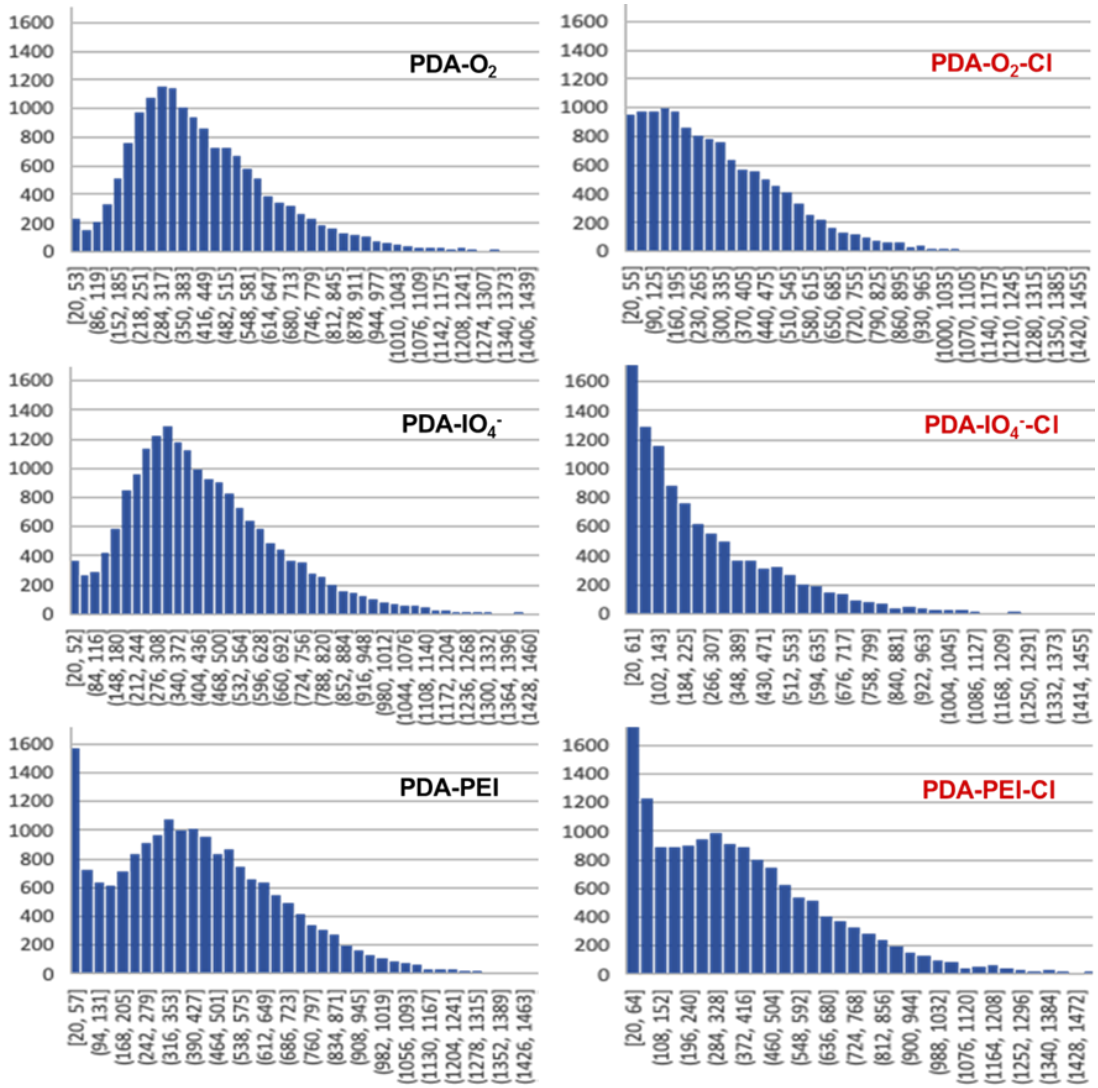

Figure 7. Size distribution (on pixels) of adhered *E. coli* on PDA-X and PDA-X-Cl coatings, observed by optical microscopy with green epifluorescence staining (Syto™ 9).

In addition, we have noticed during our experiments that fluorescent intensity was varying a lot when passing from the PDA coatings to the chlorinated ones, without any experimental condition changes. Therefore, we have carried out statistical analyses on the size of bacteria by average the numbers of pixels observed for each single bacterium. The data are presented in Figure 7. It is quite clear that on non-chlorinated surfaces, the size distribution of adhered bacteria is as often observed with a Poisson distribution profile with a clear apex observed. However, when looking at the shape of this distribution for chlorinated films, it is clear that the size distribution has changed, with no more Poisson distribution profile, and a net decrease of the size of the bacteria. This size decrease was also observed by scanning electron microscopy, Figure 8. The average size of *E. coli* is around 1.5-1.9 µm for PDA-O_2 films, while the average size is closer to 0.8-1.2 µm when the film has been chlorinated. Moreover, the shape of the bacteria is also affected, with no longer a clear elongated bacillus shape but rather an oval one.

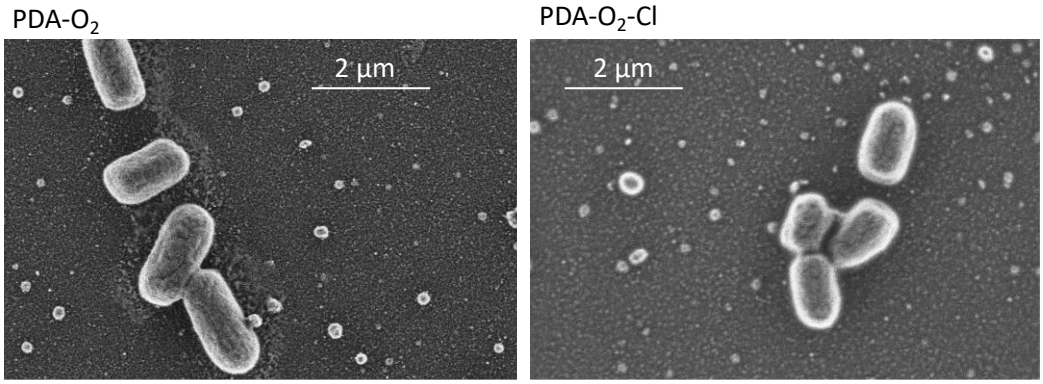

Figure 8. SEM micrographs of *E. coli* on PDA-O_2 (left) and PDA-O_2-Cl (right) coatings.

The following experiments were carried out using an indirect method consisting on recovering adhered bacteria from a given surface (either by mild sonication or by vortexing) and to count the number of viable bacteria, after deposition/growth of recovered bacteria on agar plates. The data obtained on agar plates are shown in Figure S8 and Table S1, the results are summarized in Table 4. For each chlorinated surface, two references were used to calculate the *%killing*, either the initial concentration of the bacterial inoculum or by taking into account the respective non-chlorinated surface, using equation (4).

Table 4. Killing percentage *(%killing)* of chlorinated coating obtained from CFU numbering on agar plates referenced towards the bacterial inoculum and towards the non-chlorinated coatings.

	PDA-Cl		PDA-IO_4^--Cl		PDA-PEI-Cl	
Reference	Inoculum	PDA	Inoculum	PDA-IO_4^-	Inoculum	PDA-PEI
E. coli ATCC 25922	99.0	34.0	97.7	91.4	97.4	86.2
S. epidermidis CIP 6821	70.0	59.4	83.0	76.6	66.6	58.7

When looking at results obtained for *E. coli*, and when comparing to the initial bacterial inoculum, all three PDA-chlorinated surfaces enables an inactivation of bacterial viability close to 2 log reduction, with the values ranging from 97.4% to 99.0%, as already observed for PDA-O_2 in our previous study [26]. When comparing now with the non-chlorinated surface, these *%killing* are varying quite a lot as a function of the considered surface. In fact, for the classical PDA-O_2-Cl, the *%killing* is only 34%, while both PDA-IO_4^--Cl and PDA-PEI-Cl exhibit *%killing* higher than 86%. In the case of PDA-IO_4^-Cl, this difference can be explained by the fact that the film is thicker. However, at the point it should be noted that I atoms could also participate to the antibacterial properties of this PDA film. In the case of PDA-PEI, it can be explained by the fact that more NH groups are available for chlorination (see XPS data of Tables 1 and 2) with overall more N-Cl functions available.

The tendencies are more or less the same when looking at the data obtained for *S. epidermidis*, with higher *%killing* of the chlorinated films when referenced to the inoculum than referenced with the non-chlorinated coatings. However lower killing efficiencies observed towards *S. epidermidis* are observed compared to those observed for *E. coli*. That could be explained by the composition of the bacterial membrane of Gram positive bacteria, as already observed by Targosz *et al.* [55], with an enriched peptidoglycan concentration for Gram positive bacteria. Nonetheless, a coating seems to have better efficiency than the others two: PDA-IO_4^-Cl, further experiments should be conducted to specify the rule of the iodine atoms immobilized on/in the PDA coating

4. Discussion

In this work, we studied the optimization of the antibacterial response of *N*-halamine coatings based on PDA film. As reminder, a previous study demonstrated the elaboration of a new antibacterial coating formed by a thin chlorinated PDA film containing chloramine functions inside the polymer. The amount of these functions was estimated between 10^{21} and 10^{22} at cm^{-3} [26] giving, for chlorinated PDA coatings, a *E. coli* adhesion reduction up to 45% compared to uncoated surfaces and a bacterial viability reduction of 99% on chlorinated PDA coating compared to initial inoculum concentration and 34% when compared to the non-chlorinated PDA film.

In order to optimize the amount of haloamine functions available on/in the material to be protected, we have studied other PDA deposition pathways that make it possible to increase the amount of amine functions. For this, two additional routes were considered. The first one was to accelerate the kinetics of PDA film formation by using a more powerful oxidant, *ca.* sodium periodate, and increasing the thickness of the deposit that reachs 100 nm after 24 h. However, the PDA coating is rough and iodine atoms remain trapped on/in the coating. The second route consisted of the use of a second polymer richer in amine functions, PEI. PEI is known to act as a crosslinker within the structure of PDA thus allowing more stable coatings to be obtained. The PM-RAIRS analyzes confirmed the deposition of the composite and the XPS measurements showed an enrichment of the PDA-PEI coating in amine functions.

The chlorination of the different PDA films was carried out using diluted NaOCl as a function of contact time and concentration in order to optimize the chlorination process. According to XPS analysis, probing the extreme film surface, we have concluded that the efficiency of chlorination was the best for the PDA-O_2 films with more than 60% of the N atoms that are chlorinated, while this value is only 30% for the two other films. These differences between the PDA-O_2, PDA-IO_4^- and PDA-PEI coatings can be explained by the availability of N-H function. Indeed, the PDA-IO_4^- coating is composed by different hyperoxidized structure compared to the PDA-O_2 film, with a higher proportion of tertiary amine functions for which no chlorination is possible. For the PDA-PEI coating, NH_2 functions can be engaged in hydrogen bonds with the adjacent catechol functions which do not allow the chlorination. The chlorination quantification of the whole films was carried out by chemical assay with TNB and revealed that the PDA-PEI film showed the higher density of N-Cl groups, which is not the one having the higher N/Cl ratio. The three films of PDA exhibit high amount of chlorine, ranging from $5x10^{20}$ to almost 10^{22} atoms per cm^3. We noticed difference between XPS results and chemical assay with TNB coming first of all from the fact that a quantification technique is used here which probes the depth of the fim, unlike the XPS analysis which only provides information on the film surface. Moreover, due to the nature of the PDA-IO_4^- coating which are rougher and denser than the PDA-O_2 coating, the diffusion of the TNB molecules through the entire thickness of the coatings could be difficult.

Next, the efficiency of the unchlorinated and chlorinated coatings in eliminating two different bacterial strains: one Gram negative bacteria, *Staphylococcus epidermidis* CIP 6821, and one Gram negative bacteria, *Escherichia coli* ATCC 25922, was studied. The first test was carried out following a direct experiment by optical microscopy using fluorescent stains to evaluate the bacterial adherence and the cell mortality. For *E. coli*, all chlorinated surfaces exhibited a lower number of bacteria compared to the respective non-chlorinated surfaces. For PDA-O_2 and PDA-IO_4^-, the net decrease of bacterial adherence was 25% and 38% respectively. Concerning the PDA-PEI surface, a decrease of 21% was observed but with no significant difference ($p > 0.01$). Surprisingly, for *S. epidermidis* bacterial strain all the adherences recorded showed no statistically significant difference, this finding could be explained by the composition of the membrane of Gram positive with the presence of charged liposaccharides and peptidoglycans [55]. Moreover, PDA-PEI surface exhibited a much lower adherence with 36% less adhered bacteria compared to the chlorinated film. This result could be due again to the positive charges present on the outer membrane of

S. epidermidis bacteria, resulting on charged repulsion between these ones and the positively charged amine groups of PEI.

Following the evaluation of adherence properties, the killing properties of surface were evaluated. Bad killing efficiency was obtained with this technique for all the tested PDA surfaces. We can notice that the live/dead fluorescent technique is very efficient when the damages caused to the bacteria by the antibacterial agents affect directly the integrity of the membrane of the bacteria. Thus, the mode of actions of haloamine moieties seems to be more directed towards growth inhibition by blocking the cellular division rather than membrane disruption, that could explain the poor number of red bacteria observed during our fluorescent optical microscopy experiments. This was confirmed by a statistical analysis of the size of bacteria grown on chlorinated film, looking at the shape of this distribution it is clear that the bacteria size has changed with a net increase of the number of small bacteria. In fact, the average size of *E. coli* that have adhered on chlorinated PDA film were one third of the ones adhered on un-chlorinated PDA film. Moreover, the shape of the bacteria was also affected, with an oval shape.

A second indirect route was based on the recovery of adhered bacteria and viable cell culture counting on agar plates. When looking at results obtained for *E. coli*, and when comparing to the initial bacterial inoculum, the three chlorinated PDA surfaces enable an inactivation of bacterial viability close to 2 log reduction, with the values ranging from 97.4% to 99.0%, as already observed for PDA-O_2 in our previous study [26]. However when comparing with the non-chlorinated surface, for the classical PDA-O_2-Cl film, the *%killing* is only 34%, while PDA-IO_4^--Cl and PDA-PEI-Cl films exhibit *%killing* higher than 86%. These differences can be explained, in the case of PDA-IO_4^-Cl, by a thicker and more dense film (Figures S2 and S3), rendering the haloamine functions more accessible for antibacterial activity. In the case of PDA-PEI, it can be explained by the fact that more NH groups are available for chlorination with overall more N-Cl functions available. The tendencies were quite similar for *S. epidermidis*, with higher *%killing* of the chlorinated films when referenced to the inoculum than referenced with the non-chlorinated coatings. However lower killing efficiencies were observed towards *S. epidermidis* compared to those for *E. coli*, and that could be again explained by the composition of the bacterial membrane.

5. Conclusions

To conclude, we have shown in this study how to elaborate several PDA-based antibacterial coatings composed of thin *N*-halamine films. Three routes have been followed, a "classical" one with PDA formed with TRIS in the presence of atmospheric O_2. A second route was obtained by changing the oxidizing agent by replacing the atmospheric O_2 by a stronger oxidant agent, $NaIO_4$, finally a copolymer PDA-PEI using the conditions of the "classical" route. The three coatings exhibit similar haloamine concentration in the order of 2.5×10^{21} and 9×10^{21} Cl at·cm^{-3} for PDA-O_2 and PDA-PEI, respectively. Noteworthy, for PDA-IO_4^- coatings, the Cl(+I) density is four times lower. Microbiological tests were carried out on two bacterial strains *E. coli* and *S. epidermidis*. Direct tests, fluorescent staining observed by optical microscopy, have revealed a clear decrease of bacterial adherence for *E. coli*, up to 40%, while no statistical decrease was observed for *S. epidermidis*. In addition, these direct tests have shown that the morphology of bacteria after contact with *N*-halamine coating has changed, with smaller size and distorted shape. Indirect tests evidenced differences on the viability/growth of adhered bacteria, with bactericidal properties higher in the case of Gram negative bacteria than for Gram positive bacteria. The reduction of viable bacteria is higher when compared to the initial inoculum rather than compared to the non-chlorinated surfaces. Finally, for both bacterial strains, the best PDA coating appears to be the PDA-IO_4^-Cl one, especially when considering that it contains four times less active haloamine functions for a 25% better bactericidal efficiency.

Supplementary Materials: The following are available online at www.mdpi.com/xxx/s1, **Figure S1.** PM-RAIRS spectra of gold surfaces coated with PDA-O_2, PDA-IO_4^- *and* PDA-PEI films. **Figure S2.** PDA-O_2, PDA-IO_4^- and PDA-PEI film thickness evaluated by SEM observations and ellipsometry measurements. **Figure S3.** SEM micrographs of PDA-O_2, PDA-IO_4^- and PDA-PEI coatings on gold substrate. **Figure S4.** Evolution of the contact angle with water for PDA-O_2, PDA-IO_4^- and PDA-PEI coatings. **Figure S5.** Representative structural components in PDA-IO_4^- and PDA-PEI films. **Figure S6.** Numbering of chloramine functions by TNB. **Figure S7.** Statistical analyses of bacterial adherence. **Figure S8** Optical photographs of agar plates presenting the killing tests results. **Table S1** Average number of bacteria, in CFU.mL^{-1}, after killing tests against the different PDA coatings.

Author Contributions: Conceptualization, C.D.C. and V.H.; methodology, C.D.C. and V.H.; validation, C.D.C. and V.H.; formal analysis, N.N. and A.M.; investigation, N.N and A.M. ; writing—original draft preparation, N.N, A.M., C.D.C. and V.H.; writing—review and editing, N.N, A.M., C.D.C. and V.H.; supervision, C.D.C. and V.H.; funding acquisition, C.D.C. and V.H.

All authors have read and agreed to the published version of the manuscript.

Funding: A. M. would like to thanks the European cross-border cooperation program Interreg Franco-Suisse 2014-2020 and the FEDER agency (*Fonds européen de développement régional*) for fundings. This work was also supported by French state funds managed by the ANR within the *Investissements d'Avenir* program under reference ANR-11-IDEX-0004-02 and more specifically within the framework of the Cluster of Excellence MATISSE, which provided experimental support funding for N.N. This work was partly supported by the French Renatech network and its FEMTO-ST technological facility (SEM-FEG Imaging).

Acknowledgments: The authors acknowledge IMPC (Institut des Matériaux de Paris Centre, FR2482) and the C'Nano project of Region Ile-de-France, for Omicron XPS apparatus funding. A.M and V.H. would like to thanks Marina Raschetti for her help in setting up the experiments with SEM-FEG.

Conflicts of Interest: "The authors declare no conflict of interest."

References

1. de Carvalho, C. C. C. R. Marine Biofilms: A Successful Microbial Strategy With Economic Implications. *Front Mar Sci* **2018**, *5*, 126.

2. Hall-Stoodley, L.; Costerton, J. W.; Stoodley, P. Bacterial biofilms: from the Natural environment to infectious diseases. *Nat Rev Microbiol* **2004**, *2*, 95-108.

3. Nickel, J. C.; Ruseska, I.; Wright, J. B.; Costerton, J. W. Tobramycin resistance of Pseudomonas aeruginosa cells growing as a biofilm on urinary catheter material. *Antimicrob Agents Chemother* **1985**, *27*, 619-624.

4. Rabin, N.; Zheng, Y.; Opoku-Temeng, C.; Du, Y.; Bonsu, E.; Sintim, H. O. Biofilm formation mechanisms and targets for developing antibiofilm agents. *Future Med Chem* **2015**, *7*, 493-512.

5. Veerachamy, S.; Yarlagadda, T.; Manivasagam, G.; Yarlagadda, P. K. Bacterial adherence and biofilm formation on medical implants: a review. *Proc Inst Mech Eng H* **2014**, *228*, 1083-99.

6. Donlan, R. M. Biofilms: microbial life on surfaces. *Emerg Infect Dis* **2002**, *8*, 881-90.

7. Dufour, D.; Leung, V.; Lévesque, C. M. Bacterial biofilm: structure, function, and antimicrobial resistance. *Endod Topics* **2010**, *22*, 2-16.

8. Alves, D.; Pereira, M. O. Mini-review: Antimicrobial peptides and enzymes as promising candidates to functionalize biomaterial surfaces. *Biofouling* **2014**, *30*, 483-499.

9. Chen, J.; Zhu, Y.; Xiong, M.; Hu, G.; Zhan, J.; Li, T.; Wang, L.; Wang, Y. Antimicrobial Titanium Surface via Click-Immobilization of Peptide and Its in Vitro/Vivo Activity. *ACS Biomater Sci Eng* **2019**, *5*, 1034-1044.

10. Cox, H. J.; Li, J.; Saini, P.; Paterson, J. R.; Sharples, G. J.; Badyal, J. P. S. Bioinspired and eco-friendly high efficacy cinnamaldehyde antibacterial surfaces. *J Mater Chem B* **2021**, *9*, 2918-2930.

11. Nicolas, M.; Beito, B.; Oliveira, M.; Tudela Martins, M.; Gallas, B.; Salmain, M.; Boujday, S.; Humblot, V. Strategies for Antimicrobial Peptides Immobilization on Surfaces to Prevent Biofilm Growth on Biomedical Devices. *Antibiotics* **2022**, *11*, 13.
12. Shahnawaz Khan, M.; Abdelhamid, H. N.; Wu, H.-F. Near infrared (NIR) laser mediated surface activation of graphene oxide nanoflakes for efficient antibacterial, antifungal and wound healing treatment. *Colloids Surf B: Biointerfaces* **2015**, *127*, 281-291.
13. Siedenbiedel, F.; Tiller, J. Antimicrobial Polymers in Solution and on Surfaces: Overview and Functional Principles. *Polymers* **2012**, *4*, 46-71.
14. Fan, X.; Ren, X.; Huang, T.-S.; Sun, Y. Cytocompatible antibacterial fibrous membranes based on poly(3-hydroxybutyrate-co-4-hydroxybutyrate) and quaternarized N-halamine polymer. *RSC Advances* **2016**, *6*, 42600-42610.
15. Kügler, R.; Bouloussa, O.; Rondelez, F. Evidence of a charge-density threshold for optimum efficiency of biocidal cationic surfaces. *Microbiology* **2005**, *151*, 1341-1348.
16. Olsen, I. Biofilm-specific antibiotic tolerance and resistance. *Eur J Clin Microbiol Infect Dis* **2015**, *34*, 877-886.
17. Olson, M. E.; Ceri, H.; Morck, D. W.; Buret, A. G.; Read, R. R. Biofilm bacteria: formation and comparative susceptibility to antibiotics. *Can J Vet Res* **2002**, *66*, 86-92.
18. Timofeeva, L.; Kleshcheva, N. Antimicrobial polymers: mechanism of action, factors of activity, and applications. *Appl Microbiol Biotechnol* **2011**, *89*, 475-492.
19. Baltzer, S. A.; Brown, M. H. Antimicrobial peptides: promising alternatives to conventional antibiotics. *J Mol Microbiol Biotechnol* **2011**, *20*, 228-35.
20. Bang, S. H.; Sekhon, S. S.; Ahn, J.-Y.; Kim, Y.-H.; Min, J. Advances in antimicrobial agents based lysosomes. *Mol Cell Toxicol* **2014**, *10*, 229-235.
21. Bechinger, B.; Gorr, S. U. Antimicrobial Peptides: Mechanisms of Action and Resistance. *J Dent Res* **2017**, *96*, 254-260.
22. Harris, F.; Dennison, S. R.; Phoenix, D. A. Anionic antimicrobial peptides from eukaryotic organisms. *Curr Protein Pept Sci* **2009**, *10*, 585-606.
23. Shima, S.; Matsuoka, H.; Iwamoto, T.; Sakai, H. Antimicrobial action of epsilon-poly-L-lysine. *J Antibiot* **1984**, *37*, 1449-55.
24. Dong, A.; Wang, Y.-J.; Gao, Y.; Gao, T.; Gao, G. Chemical Insights into Antibacterial N-Halamines. *Chem Rev* **2017**, *117*, 4806-4862.
25. Hui, F.; Debiemme-Chouvy, C. Antimicrobial N-Halamine Polymers and Coatings: A Review of Their Synthesis, Characterization, and Applications. *Biomacromolecules* **2013**, *14*, 585-601.
26. Nazi, N.; Humblot, V.; Debiemme-Chouvy, C. A New Antibacterial N-Halamine Coating Based on Polydopamine. *Langmuir* **2020**, *36*, 11005-11014.
27. Chien, H.-W.; Chiu, T.-H. Stable N-halamine on polydopamine coating for high antimicrobial efficiency. *Eur Polym J* **2020**, *130*, 109654.
28. Liu, Y.; Ai, K.; Lu, L. Polydopamine and its derivative materials: synthesis and promising applications in energy, environmental, and biomedical fields. *Chem Rev* **2014**, *114*, 5057-115.
29. Ye, Q.; Zhou, F.; Liu, W. Bioinspired catecholic chemistry for surface modification. *Chem Soc Rev* **2011**, *40*, 4244-58.
30. Ball, V. Physicochemical perspective on "polydopamine" and "poly(catecholamine)" films for their applications in biomaterial coatings. *Biointerphases* **2014**, *9*, 030801.
31. Ponzio, F.; Ball, V. Polydopamine deposition at fluid interfaces. *Polym Int* **2016**, *65*, 1251-1257.
32. Ponzio, F.; Barthès, J.; Bour, J.; Michel, M.; Bertani, P.; Hemmerlé, J.; d'Ischia, M.; Ball, V. Oxidant Control of Polydopamine Surface Chemistry in Acids: A Mechanism-Based Entry to Superhydrophilic-Superoleophobic Coatings. *Chem Mater* **2016**, *28*, 4697-4705.
33. Lv, Y.; Yang, S.-J.; Du, Y.; Yang, H.-C.; Xu, Z.-K. Co-deposition Kinetics of Polydopamine/Polyethyleneimine Coatings: Effects of Solution Composition and Substrate Surface. *Langmuir* **2018**, *34*, 13123-13131.
34. Chien, H. W.; Chiu, T. H.; Lee, Y. L. Rapid Biocidal Activity of N-Halamine-Functionalized Polydopamine and Polyethylene Imine Coatings. *Langmuir* **2021**, *37*, 8037-8044.

35. Humblot, V.; Yala, J.-F.; Thebault, P.; Boukerma, K.; Hequet, A.; Berjeaud, J.-M.; Pradier, C.-M. The antibacterial activity of Magainin I immobilized onto mixed thiols Self-Assembled Monolayers. *Biomaterials* **2009**, *30*, 3503-3512.
36. Lee, B. P.; Messersmith, P. B.; Israelachvili, J. N.; Waite, J. H. Mussel-Inspired Adhesives and Coatings. *Annu Rev Mater Res* **2011**, *41*, 99-132.
37. Lee, H.; Dellatore, S. M.; Miller, W. M.; Messersmith, P. B. Mussel-Inspired Surface Chemistry for Multifunctional Coatings. *Science* **2007**, *318*, 426-430.
38. Del Frari, D.; Bour, J.; Ball, V.; Toniazzo, V.; Ruch, D. Degradation of polydopamine coatings by sodium hypochlorite: A process depending on the substrate and the film synthesis method. *Polym Degrad Stab* **2012**, *97*, 1844-1849.
39. Ma, K.; Jiang, Z.; Li, L.; Liu, Y.; Ren, X.; Huang, T.-S. N-halamine modified polyester fabrics: Preparation and biocidal functions. *Fibers Polym* **2014**, *15*, 2340-2344.
40. Scofield, J. H. Hartree-Slater Subshell Photoionization Cross-Sections at 1254 and 1487 eV. *J Elec Spectrosc Relat Phenom* **1976**, *8*, 129-137.
41. Riddles, P. W.; Blakeley, R. L.; Zerner, B. Ellman's reagent: 5,5′-dithiobis(2-nitrobenzoic acid) a reexamination. *Anal Biochem* **1979**, *94*, 75-81.
42. Debiemme-Chouvy, C.; Haskouri, S.; Folcher, G.; Cachet, H. An Original Route to Immobilize an Organic Biocide onto a Transparent Tin Dioxide Electrode. *Langmuir* **2007**, *23*, 3873-3879.
43. Segut, O.; Herlem, G.; Lakard, B.; Blondeau-Patissier, V.; Nardin, M.; Gree, S.; Rauch, J.-Y. Electrochemically deposited polyethyleneimine films and their characterization. *Synth Met* **2010**, *160*, 1359-1364.
44. Zangmeister, R. A.; Morris, T. A.; Tarlov, M. J. Characterization of Polydopamine Thin Films Deposited at Short Times by Autoxidation of Dopamine. *Langmuir* **2013**, *29*, 8619-8628.
45. Chen, T.-P.; Liu, T.; Su, T.-L.; Liang, J. Self-Polymerization of Dopamine in Acidic Environments without Oxygen. *Langmuir* **2017**, *33*, 5863-5871.
46. Jiang, J.; Zhu, L.; Zhu, L.; Zhu, B.; Xu, Y. Surface characteristics of a self-polymerized dopamine coating deposited on hydrophobic polymer films. *Langmuir* **2011**, *27*, 14180-14187.
47. Zheng, W.; Fan, H.; Wang, L.; Jin, Z. Oxidative Self-Polymerization of Dopamine in an Acidic Environment. *Langmuir* **2015**, *31*, 11671-11677.
48. Weidman, S. W.; Kaiser, E. T. The Mechanism of the Periodate Oxidation of Aromatic Systems. III. A Kinetic Study of the Periodate Oxidation of Catechol. *J Am Chem Soc* **1966**, *88*, 5820-5827.
49. Alfieri, M. L.; Panzella, L.; Oscurato, S. L.; Salvatore, M.; Avolio, R.; Errico, M. E.; Maddalena, P.; Napolitano, A.; D'Ischia, M. The Chemistry of Polydopamine Film Formation: The Amine-Quinone Interplay. *Biomimetics* **2018**, *3*, 26.
50. Tanuma, S.; Powell, C. J.; Penn, D. R. Calculation of electron inelastic mean free paths (IMFPs) VII. Reliability of the TPP-2M IMFP predictive equation. *Surf Interface Anal* **2003**, *35*, 268-275.
51. Xu, L.; Zuo, Y. Y. Reversible Phase Transitions in the Phospholipid Monolayer. *Langmuir* **2018**, *34*, 8694-8700.
52. Yang, W.; Liu, C.; Chen, Y. Stability of Polydopamine Coatings on Gold Substrates Inspected by Surface Plasmon Resonance Imaging. *Langmuir* **2018**, *34*, 3565-3571.
53. Curtis, K. A.; Miller, D.; Millard, P.; Basu, S.; Horkay, F.; Chandran, P. L. Unusual Salt and pH Induced Changes in Polyethylenimine Solutions. *PLoS ONE* **2016**, *11*, e0158147.
54. Luo, J.; Chen, Z.; Sun, Y. Controlling biofilm formation with an N-halamine-based polymeric additive. *J Biomed Mater Res* **2006**, *77A*, 823-831.
55. Marcinkiewicz, J.; Biedroń, R.; Białecka, A.; Kasprowicz, A.; Mak, M.; Targosz, M. Susceptibility of Propionibacterium acnes and Staphylococcus epidermidis to killing by MPO-halide system products. Implication for taurine bromamine as a new candidate for topical therapy in treating acne vulgaris. *Arch Immunol Ther Exp* **2006**, *54*, 61-68.